(This is a sample cover image for this issue. The actual cover is not yet available at this time.)

Journal of African Earth Sciences 61 (2011) 273–285

Contents lists available at SciVerse ScienceDirect

Journal of African Earth Sciences

journal homepage: www.elsevier.com/locate/jafrearsci

Micro-Raman spectroscopy of gem-quality chrysoprase from the Biga–Çanakkale region of Turkey

Murat Hatipoğlu [a,b,*], Ufuk Ören [b], Yaşar Kibici [c]

[a] Dokuz Eylül University, IMYO, Izmir Multidisciplinary Vocational School, Gemmology and Jewellery Programme, TR-35380 Buca-İzmir, Turkey
[b] Dokuz Eylül University, The Graduate School of Natural and Applied Sciences, Department of Natural Building Stones and Gem Stones, TR-35370 Buca-İzmir, Turkey
[c] Dumlupınar University, Faculty of Engineering, Department of Geological Engineering, TR-43100 Kampüs-Kütahya, Turkey

ARTICLE INFO

Article history:
Received 17 February 2011
Received in revised form 7 August 2011
Accepted 19 August 2011
Available online 14 September 2011

Keywords:
Chrysoprase
Chalcedonic-quartz
Dispersive confocal micro-Raman spectroscopy (DCμRS)
Biga-Çanakkale region
Turkey

ABSTRACT

The commercial quantities of gem-quality dark green chrysoprase are found as the fracture fillings covered with a weathering crust in the silicified serpentinites throughout the border of a metamorphic zone in the Biga–Çanakkale region of Turkey. However, the green-stained opaque quartz materials are also present in the same deposit, but these materials are common and in low-demand according to chrysoprase in terms of gemmological importance. Thus, it is necessary to distinguish these two similar materials from each other non-destructively. In addition, all chrysoprase roughs in this deposit also have alpha-quartz and moganite inclusions. Accordingly, dispersive (visible) confocal micro-Raman spectroscopy (DCμRS) allows us to distinguish clearly the chalcedonic-quartz silica phase (fibrous quartz (chalcedony)) from the crystalline-quartz silica phase (fine-grained alpha-quartz) in the case of both quartz inclusions in the chrysoprase material and itself of the green-stained quartz material in the same deposit.

This study characterizes the Biga chrysoprase (Turkey) in terms of silica building phases, chemical content, and individual Raman bands, using several destructive and non-destructive analytical techniques.

The Raman spectra show that the most characteristic intensive and the widest Raman bands peaked at about 498 and 460 cm^{-1} can be inferred to ν_2 doubly symmetric bending mode of [SiO_4/M] centers. The "M" includes the some cationic substitutions of Si by Fe, Cr, Mn, As, Ni, Pb, Sb, and Zn, and K and Na as well. The second characteristic Raman band peaked at about 206 cm^{-1} can be inferred to single translational libration mode. The last readable Raman bands peaked at about 139 and 126 cm^{-1} can be inferred to doubly translational libration modes as well. In addition, the weaker Raman bands peaked at about 1577, 1430, 1303, 1160, 1082, 549, 394, 352, and 259 cm^{-1} are also present.

As a result, the dispersive confocal micro-Raman spectrum of chrysoprase is directly related to its silica building phases and trace element implications.

1. Introduction

Chrysoprase is a dark and/or light green-colored sub-variety of the microcrystalline quartz group (Rossman, 1994; Back and Mandarino, 2008). The material is micro fibrous, and sometimes contains fine-grained silica (Frondel, 1978). Chrysoprase is in high-demand in terms of gemmological importance (Arem, 1987).

Since chrysoprase was firstly identified in the 18th century in the region of Lower Silesia in Szklary near Zabkowice Slaskie in Poland (Sachanbinski et al., 2001), today, the worldwide commercial deposits of chrysoprase are still found rarely. Besides, the deposits are mainly located in Australia (Nagase et al., 1997; Befi, 2009), Poland (Sachanbinski et al., 2001; Skrzypek et al., 2003, 2004), Kazakhstan (Sachanbinski et al., 2001; Witkowski and Zabinski, 2004), Brazil (Komov et al., 1994), Tanzania (Witkowski and Zabinski, 2004; Shigley et al., 2009), and Turkey as well.

On the other hand, chrysoprase has been worked as many architectural objects (artifacts) since the ancient times. For instance, chrysoprase was very popular in the 14th century when the Holy Roman Emperor Charles IV used it to decorate chapels, including the Chapel of Saint Wenceslas in Prague (Sachanbinski et al., 2001). It is well-known that some chrysoprase pits near the village of Dikmen in the Biga–Çanakkale region of Turkey (Fig. 1) have been mined since the Ottoman Empire Period (from the least 1700s to now). During the field investigation, these pits have been observed as good-conserved (Fig. 2). Furthermore, some of the chrysoprase samples collected from this pits were cut and polished into cabochons and slabs as gem objects. It is revealed that the objects display the typical green color and the gem quality of the chrysoprase material (Fig. 3).

* Corresponding author at: Dokuz Eylül University, IMYO, Izmir Multidisciplinary Vocational School, Gemmology and Jewellery Programme, TR-35380 Buca-İzmir, Turkey. Tel.: +90 232 4400707x107.
E-mail address: murat.hatipoglu@deu.edu.tr (M. Hatipoğlu).

1464-343X/$ - see front matter © 2011 Elsevier Ltd. All rights reserved.
doi:10.1016/j.jafrearsci.2011.08.002

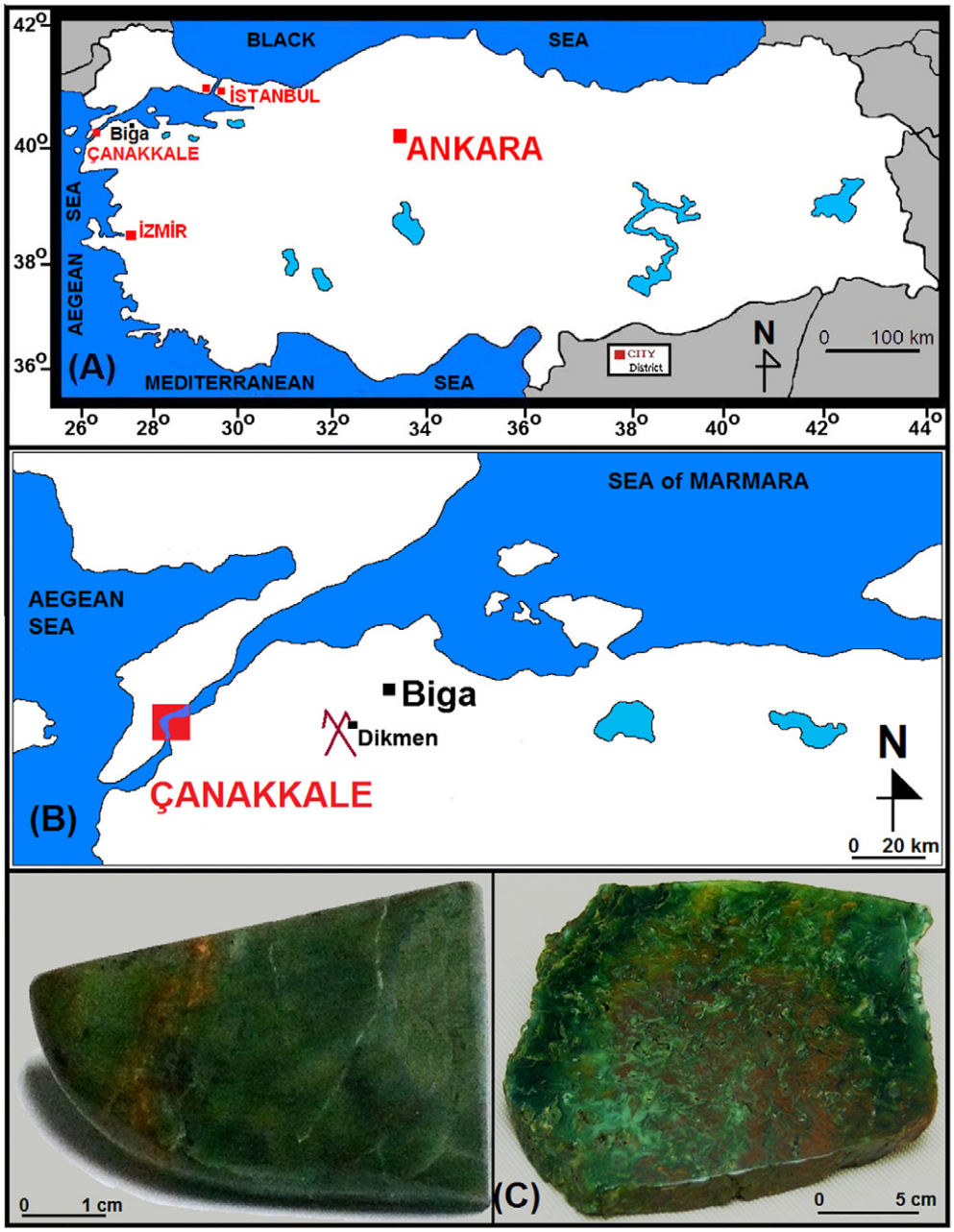

Fig. 1. Location map showing the Biga-Çanakkale region in Turkey (A), and enlarged map comprising the village of Dikmen in the Biga–Çanakkale region, where the commercial quantities of gem-quality massive chrysoprase masses are located (B). Two representative Biga chrysoprase gem objects were cut and polished (C). The chrysoprase material is often interlaced with a brownish crust of ferric hydroxide.

In the large scale, the Biga Peninsula comprising whole Biga–Çanakkale region as well as the village of Dikmen nearby chrysoprase depositional field is geologically described in detail some authors (Bingöl et al., 1973; Okay et al., 1991; Okay and Satır, 2000; Koçyiğit et al., 2006). They has been importantly reported that there is a major NE–SW trending tectonic belt running from the district of Karabiga to the district of Ezine, which characterizes the region. We also have seen that the chrysoprase bearing zone in the region is on this tectonic belt.

On the other hand, It has been stated by many authors that the massive-structured chrysoprase materials can be confused with the massive-structured green-stained opal and quartz materials in the chrysoprase mines in the world (Arem, 1987; Shigley et al., 2009), since chrysoprase-bearing serpantinitic masses can contain the mixing of prasopal, green quartz, and some nickel- and magnesium-rich minerals (Caillaud et al., 2009; Shigley et al., 2009). Therefore, it is still an important problem to distinguish these similar colored silica varieties non-destructively on gem market.

After the Raman effect was firstly predicted by Smekal in 1923, and later observed experimentally by Raman and Krishnan in 1928 (Raman, 1928), FT-Raman spectroscopy and/or Dispersive(Vis)-Raman spectroscopy have been used as the important spectroscopic techniques in the condensed matter physics and chemistry to study vibrational, rotational, and other low-frequency modes in a system (Deckert et al., 2008; Gucsik, 2009; Vandenabeele, 2010). The frequency wavenumber of the Raman scattering signal is a reflection of the vibration and rotational modes of the molecule (Lewis and Edwards, 2001; Slodczyk and Colomban, 2010; Vandenabeele, 2010). Raman maps are the images generated from spectra

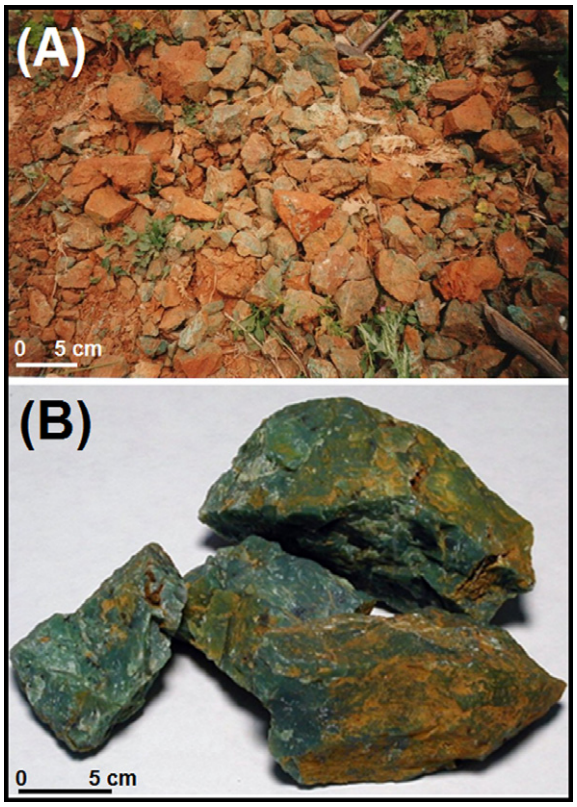

Fig. 2. Commercial quantities of gem-quality dark green chrysoprase masses are found as the fracture fillings in the silicified serpentinite cracks throughout the border of the metamorphic zone near the village of Dikmen, in the district of Biga in the province of Çanakkale (Turkey). The dimensions of the samples occurring as fracture fillings vary according to the size of the cracks (A). Thus, they are massive-structured irregular masses covered with a weathering crust, which vary in size from small (about 1 cm in thickness) to giant (about 50 cm in thickness) (B).

recorded at discrete points of the sample (the recording is automated). They show the variation of any fitted parameter (i.e. intensity, width or position of one band) as a function of the point of analysis. If the mapping is regular and sufficiently tight, one gets a "smart map" of the parameter (color or contrast scaling) superimposed with the optical image of the probed area. Raman mapping is very suitable for direct Raman imaging, where a large area of the sample is probed all at once and no fitting is required. More precisely, only photons from a narrow spectral domain are sent to the CCD mosaic and each pixel receives those coming from a given area of the sample. The intensity of the signal thus reveals the presence and location of any substance with a strong Raman signal in the selected spectral window (Gouadec and Colomban, 2007; Colomban and Prinsloo, 2009). The main advantages of Raman spectroscopy are its high information content, lack of sample preparation, compatibility with aqueous systems, and non-destructive nature. In addition, the spectrometer is highly suitable for further gemmological investigations of all kinds of gemstones (Bersani and Lottici, 2008; Fana et al., 2009). Thus, dispersive (visible) confocal micro-Raman spectroscopy (DCμRS) is one well-known method for the characterization and identification of the gem-minerals (Wang et al., 1994). Additionally, if required, it can be used to distinguish the similar colored materials from each other non-destructively. Thus, DCμRS can be widely applied to the identification and determination of both basic and inclusion silica building phases in gem-quality microcrystalline quartz [chalcedonic-quartzes (i.e. chrysoprase, blue chalcedony, agates, jasper, onix, and carnelian) and opalline-quartzes (i.e. fire opals, play-of-color opals, common opals, and dentritic opals)] varieties.

As a result, this study aims (1) to characterize the Biga chrysoprases (Turkey) in terms of their silica building phases, using several destructive and non-destructive analytical techniques, (2) using the dispersive confocal micro-Raman vibrational bands of the dark green chrysoprase, to distinguish clearly the chalcedonic-quartz silica building phase (fibrous quartz (length-fast chalcedony)), which is the main chrysoprase forming silica phase, from the crystalline-quartz silica phase (fine-grained alpha-quartz) in the case of both quartz inclusions in the green-colored chrysoprase material and itself of the green-stained quartz material in the same deposit, and in addition, and (3) to evaluate the possible causes of these Raman band formations in the light of polarizing microscope images, X-ray diffraction pattern, and ICP-AES chemical data.

2. Materials and methods

The investigated chrysoprase samples were obtained from the chrysoprase pits near the village of Dikmen, in the district of Biga in the province of Çanakkale (Turkey) (Fig. 1A and B). The

Fig. 3. Some polished cabochons of the Biga chrysoprases from Turkey for showing their typical color and gem quality.

Table 1
Some gemmological data of the Biga chrysoprase from Turkey according to the refractive indexes (RI), specific gravity (SG) values, and UV fluorescence reactions.

Basic gemmological data	Biga chrysoprase
Specific gravity (SG)	2.52–2.58
Refractive index (RI)	$N\omega = 1.55$ and $N\varepsilon = 1.54$
Luminescence against UV	Inert

dimensions of the chrysoprase roughs occurring as fracture fillings vary in size from small (about 1 cm in thickness) to giant (about 50 cm in thickness) according to the size of the minor cracks in the deposit (Fig. 2). Accordingly, these chrysoprase roughs are very suitable to be cut and polished for producing all kinds of gem objects (Figs. 1C and 3).

In order to verify that the investigated rough samples were indeed a silica variety, some gemmological (non-destructive) characterization tests were carried out on the many representative samples (Table 1). The tests were performed in the DGL-Gemmological Testing Laboratory at Dokuz Eylül University. Firstly, the average specific gravity (SG) values of the eight representative samples were measured using an electronic balance scale (measurement sensitivity of 0.001) with an SG kit, based on the formula ($SG = W_{air}/W_{air} - W_{water}$). The specific gravity values were obtained in the ranging between 2.52 and 2.58. Secondly, because they are opaque, the optical character, optical sign, and refractive index values of the eight representative samples were determined by the spot method, using an Eickhorst SR/XS standard refractometer device with an optical contact liquid of 1.79 RI, and a quartz lamp with a wavelength of 589 nm. The analysis shows that the samples are anisotropic, uniaxial, positive (+), and their refractive indexes (RI) are $N\omega = 1.55$ and $N\varepsilon = 1.54$; also, the double refraction (DR) = 0.01. Thirdly, ultraviolet (UV) luminescence excitation of the eight representative samples was observed using a System Eickhorst UV 240 shortwave (255 nm) and long wave (366 nm) 4 W UV lamp. As a result, the samples are inert against UV beams. Thus, when especially the specific gravity value of average 2.55 is considered beside the other verifying results, it is seen that the investigated chrysoprase samples indicate a typical chalcedonic-quartz structure, since the gem quartz varieties with the crystalline-quartz structure (i.e. amethyst, rock crystal, citrine, etc.) have a specific gravity value of about 2.65 (Back and Mandarino, 2008; Rossman, 1994; Arem, 1987).

In order to verify that the investigated rough samples were indeed a microcrystalline silica variety, some mineralogical (destructive) characterization tests were carried out on the many representative samples. Polarizing microscope images of thin sections of the investigated chrysoprase samples were obtained using an Olympus BX41 binocular polarizing microscope with a high-intensity 6 V, 30 W halogen light source combined with U-CPA and U-OPA optical systems, after thin sections of the samples had been mounted on glass lamellae. For the digital images, the microscopic magnifications (MM) are as follows; 4× (a combined magnification of 0.4× objective and 10× ocular) and 10× (a combined magnification of 1× objective and 10× ocular) under crossed nicols (+N) (active polarizer and analyzer). Polarizing microscope investigations were performed in the Optical Mineralogy Laboratory of the Department of Geology at the Dokuz Eylül University.

The base silica building components of the representative chrysoprase samples were detected using X-ray powder diffraction patterns of a Cubi-XRD device with a Cu tube and a graphic monochromotor. The samples were analyzed with Cu radiation and a 0.3 mm collimator at atmospheric pressure for 10 min each, in the range between 5 and 70° 2-theta. The d-spacing [Å] diffraction matchings using the comparative matching technique are based on the positions of peaks with relative intensities [$\%(I/I_o) \geqslant 2$], 2-theta values below 70°, and a tolerance range of ±0.01. X-ray diffraction patterns were taken in the Material Research Laboratory of the Batı Anadolu Cement Factory in İzmir.

Chemical analyses of the representative chrysoprase samples utilized the X-ray fluorescence (XRF) for major oxides, the inductively coupled plasma-atomic emission spectroscopy (ICP-AES) for trace elements, and the WST-SIM for determination of the ignition losses. These analyses were performed, and certified with the code number "IZ10048288", under contract by the accredited ALS Chemex Laboratory in Canada.

The dispersive confocal micro-Raman spectroscopy of the representative chrysoprase samples were performed on a dark background at room temperature using a HORIBA Jobin Yvan Scientific XPLORA dispersive confocal micro-Raman spectrometer (DCμRS) with a high throughput integrated spectrograph. The spectrometer uses one laser excitation of about 532 nm. Operating temperature is between 15 and 28 °C. Spectral manipulation as baseline adjustment was carried out using the software of the device. The Raman record was carried out in the DGL-Gemmological Testing Laboratory at Dokuz Eylül University.

3. Results and discussion

3.1. Provenance and genesis

The Biga Peninsula comprising whole Biga–Çanakkale region as well as the village of Dikmen nearby the current chrysoprase depositional field is an active deformational area bounded by northern Aegean Sea to the west, Dardanelles to northwest, Sea of Marmara to the north, Gulf of Edremit to southwest and the line Havran–Manyas to the east-southeast. Therefore, the Peninsula is a tectonically very active area included in the Central-northern Aegean strike-slip neotectonic domain in which the principal compressive stress is being operating in approximately *E–W* direction (Koçyiğit et al., 2006). In addition, medium-grade metamorphic rocks crop out over a large area under the Neogene sedimentary and volcanic rocks in the central Biga Peninsula in northwest Turkey (Okay and Satır, 2000). It is seen that the chrysoprase bearing zone within the ultrabasic-characterized serpentinites at the contact border of the metamorphic schists in the region is on this tectonic belt. Therefore, chrysoprase materials are mainly found as fracture fillings covered with a weathering crust in the silicified serpentinites (Fig. 2A).

As a result of the detailed field investigation, we can be stated that the chrysoprase material in the Biga–Çanakkale region (Turkey) occur due to precipitation of the silicic acid-rich dissolutions (H_4SiO_4) circulating through the several fracture zones under the ambient surrounding conditions -similar to those of the world-wide localities (Komov et al., 1994; Skrzypek et al., 2003, 2004). However, the silicic acid-rich dissolutions were firstly precipitated as the chalcedonic-quartz base silica phase [fibrous quartz (length-fast chalcedony)] throughout the outer edges of the open fractures. After then, the remainder dissolutions in the central parts of the fractures were coagulated as both the chalcedonic-quartz interval silica phase (fibrous length-slow moganite) and the crystalline-quartz silica base phase (fine-grained alpha-quartz) as inclusions depending on the temperature rising of the dissolution (Frondel, 1978; Miehe and Graetsch, 1992; Murashov and Svishchev, 1998).

Similar chrysoprase formations have been reported in many previously published papers. Accordingly, it is widely stated that the chrysoprase material can occur upon liquid–solid interactions under the ambient conditions (Nagase et al., 1997; Sachanbinski et al., 2001; Skrzypek et al., 2003, 2004; Witkowski and Zabinski, 2004; Befi, 2009; Shigley et al., 2009). The trace element contents of the chrysoprases are associated with the serpentinized and

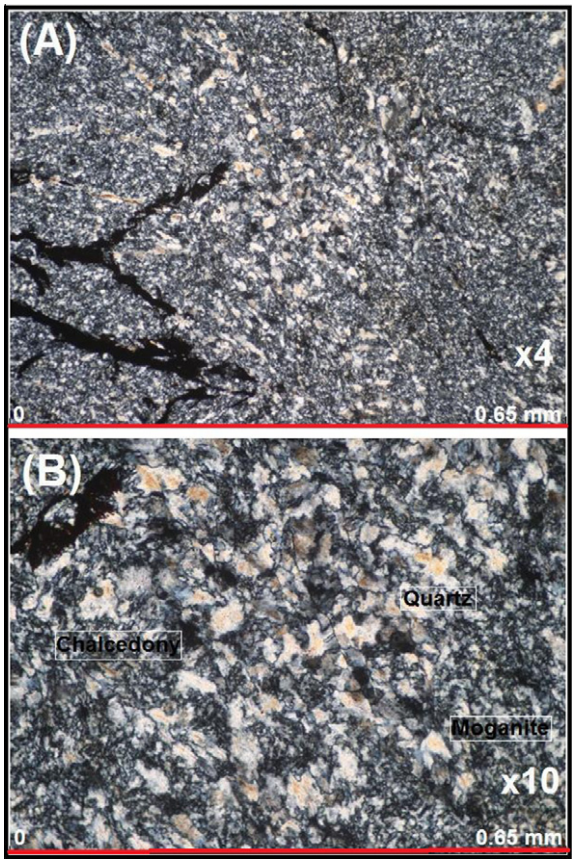

Fig. 4. Microphographs of the Biga chrysoprase, viewed in crossed-polarized light at magnifications of 4× (A) and 10× (B). It can be seen that at least 90% of the massive chrysoprase mass consists of fine radial fibrous chalcedony silica building phase with length-fast undulation (chalcedonic-quartz). The remainders were crystallized with a fine-grained alpha-quartz silica phase with length-fast undulation, and a fine radial fibrous interval moganite (or lutecite) silica phase with length-slow undulation. The width of the images is 0.65 mm.

silicified nickel- and magnesium-rich ultrabasites (Komov et al., 1994). Additionally, during the chrysoprase occurrence, mainly nickel, iron, and magnesium elements enter the silica-rich dissolution, and then migrate together with the dissolution. Finally, the independent mineral phases of nickel and nickel-magnesium hydrous silicates occur at a PH of about 6–7 (Komov et al., 1994). The most complete profiles are usually present over the weathered serpentinites, while on top of the less altered pyroxenites, there exist usually the formation of only a limonitic zone (Caillaud et al., 2009). Skrzypek and his colleagues (2004) stated that the chrysoprase samples analyzed from Poland, Kazakhstan, and Australia were formed in veins, and they were apparently associated with somewhat younger vein magnesite. In addition, their high oxygen isotope ratios suggested that the chrysoprase were precipitated from the mixed meteoric solutions in the hydrothermal conditions (Skrzypek et al., 2004).

3.2. Polarizing microscopy

The investigations of thin sections at magnifications of 4× and 10× under a polarizing microscope reveal that the Biga chrysoprases consist mainly of the micro-crystalline and macro-crystalline matrix materials (Fig. 4). Almost entire of the chrysoprase matrix contains the fibrous radial and/or bundled particles of chalcedony silica phase (fibrous quartz, optically length-fast) signing the chalcedonic-quartz silica building phase (Frondel, 1978; Miehe et al., 1984). In addition, a little of the chrysoprase matrix contains the centrally located inclusions having the fine-grained particles of alpha-quartz silica phase (fine-grained quartz, optically length-fast) and also having the fibrous radial and/or bundled particles of moganite silica phase (fibrous moganite (or lutecite, or quartzine), optically length-slow) (Miehe and Graetsch, 1992; Murashov and Svishchev, 1998). However, the coarse-grained particles of opal-CT and opal-C silica phases signing the opalline-quartz silica building phases are not observed in the chrysoprase matrix, thus it can be said that the Biga chrysoprases occur relatively higher (over 80–90 °C) formation temperature rather than worldwide localities (Skrzypek et al., 2004) (Fig. 4).

Contrary, in the chrysoprase materials found in the other locations of the world, the opalline-quartz silica building phases instead of moganite have been identified and reported. Accordingly, three mineralogical silica building phases were specified in the chrysoprases from Poland: (a) opal phases (opal-CT and opal-C)–the opal matrix contains chalcedony or quartz crystals; (b) chalcedony phase–microcrystal or fine-crystal structure, (c) chalcedony–opal phase (continuous structural transition from chalcedony crystals to quartz crystals) (Sachanbinski et al., 2001; Skrzypek et al., 2003, 2004). The silica phases in the chrysoprases from Kazakhstan have been identified as being similar to those of the chrysoprases from Poland (Sachanbinski et al., 2001; Skrzypek et al., 2003, 2004). The structure of the chrysoprases from Australia was divided into two different groups: (a) the dominant one-microcrystal quartz and fibrous chalcedony and (b) the second type: crystals of chalcedony and quartz surrounded by an opal matrix (Nagase et al., 1997; Skrzypek et al., 2004; Befi, 2009).

As a result, because of the existing of the chalcedonic-quartz silica interval phase (moganite) instead of the opalline-quartz silica base phase (opal-CT and opal-C), it can be stated that the Biga chrysoprases from Turkey occur relatively higher formation temperature conditions, and this structural feature characterize this kind of chrysoprase from the others.

3.3. X-ray diffractometry

Table 2 shows the identification of the present three different silica phases in the Biga chrysoprases, which evidence the temperature conditions during the formation of them. Accordingly, in order to verify the silica building phases in the Biga chrysoprase matrix, the numerical data obtained from the XRD analyses of the representative chrysoprase samples were matched to those of ideal crystalline-quartz, chalcedonic-quartz, and opalline-quartz silica building phases, using a comparative matching technique which were compiled from some important crystal structure databases (AMCSD, 2011; RRUFF, 2011; WEBMINERAL, 2011) and PDF cards (ASTM, 1963) as well as some previously published related papers (Miehe et al., 1984; Miehe and Graetsch, 1992; Murashov and Svishchev, 1998). The matched silica phases were labeled with specific abbreviations to help the readers as (Qu) for alpha-quartz, (Ch) for chalcedony, and (Mo) for moganite on the given X-ray diffraction pattern (Fig. 5). However, the chalcedonic-quartz silica phase (fibrous chalcedony) could not be distinguished from the crystalline-quartz silica phase (fine-grained alpha-quartz), since they exhibit the same numerical XRD data (Smith, 1997; Cady et al., 1998). Therefore, the labels belonging to fibrous chalcedony (Ch) and fine-grained alpha-quartz (Qu) were labeled on the same peaks (Fig. 5). As it can be seen in the representative XRD pattern, the Biga chrysoprases composed mainly of fibrous chalcedony and minor fibrous moganite and fine-grained alpha-quartz inclusions (Fig. 5). The XRD data of Biga chrysoprases show the lack of coarse-grained opal-CT and opal-C, which represent the opalline-quartz silica building phases of the microcrystalline quartzes (Jones and Segnit, 1971). This result

Table 2
Comparative matching of the data detected in the representative Biga chrysoprase against the ideal data of chalcedony (Ch), moganite (Mo), alpha-quartz (Qu), opal-CT (Op-CT), and opal-C (Op-C) silica building phases, using the comparative matching technique according to the d-spacing [Å] and relative intensities [%(I/I_o) ⩾ 2] of the experimental XRD numerical data. Labels are arranged according to their relative intensities. However, the chalcedonic-quartz (fibrous length-fast quartz) and crystalline-quartz (fine-grained length-fast quartz) silica phases are mixed in the XRD numerical data.

Silica phases [SiO_2]	*XRD data (ideal) [*hkl*] [Å]	XRD data (chrysoprase) [%(I/I_o) ⩾ 2]	Labels	[Å] [%(I/I_o) ⩾ 2]
Chalcedonic-Quartz Chalcedony (Ch)	[100]	4.26 (22)	Ch-Qu-Mo	4.27 (20.6)
Trigonal-Trapezohedral	[101]	3.34 (100)	Ch-Qu	3.35 (100)
Microcrystalline-	[110]	2.46 (14)	Ch-Qu	2.46 (5.8)
Cryptocrystalline	[102]	2.28 (10)	Ch-Qu-Mo	2.29 (5.9)
Fibrous, Length-fast	[111]	2.24 (5)	Ch-Qu	2.24 (2.7)
Main constitutive phase	[200]	2.13 (12)	Ch-Qu-Mo	2.13 (4.2)
	[201]	1.98 (5)	Ch-Qu	1.98 (2.7)
Crystalline-Quartz Alpha-Quartz (Qu)	[112]	1.82 (20)	Ch-Qu	1.82 (5.3)
Trigonal-Trapezohedral	[202]	1.67 (10)	Ch-Qu	1.67 (2.6)
Crystalline	[211]	1.54 (10)	Ch-Qu	1.54 (5.3)
Fine-grained, Length-fast	[203]	1.38 (7)	Mo-Ch-Qu	1.39 (5.1)
Inclusion phase	[301]	1.37 (10)	Ch-Qu	1.37 (4.7)
Chalcedonic Quartz Moganite (Mo) (or Lutecite)	[110]	4.45 (13)	Mo	–
Monoclinic-Prismatic	[−101]	4.38 (7)	Mo	–
Microcrystalline-	[002]	4.26 (5)	Ch-Qu-Mo	4.27 (20.6)
Cryptocrystalline-Interval	[−121]	3.39 (50)	Mo	–
Fibrous, Length-slow	[022]	3.33 (100)	Mo	–
Inclusion phase	[−112]	3.11 (11)	Mo	–
	[130]	2.88 (5)	Mo	–
	[−141]	2.29 (9)	Ch-Qu-Mo	2.29 (5.9)
	[123]	2.19 (5)	Mo	–
	[004]	2.13 (5)	Ch-Qu-Mo	2.13 (4.2)
	[−143]	1.83 (13)	Mo	1.83 (9.0)
	[143]	1.80 (6)	Mo	–
	[125]	1.53 (5)	Mo	1.53 (3.0)
	[−244]	1.41 (5)	Mo	–
	[−262]	1.39 (7)	Mo	1.39 (3.3)
	[145]	1.38 (11)	Mo-Ch-Qu	1.38 (5.1)
	[082]	1.28 (8)	Mo	–
	[280]	1.18 (8)	Mo	–
Opalline Quartz Opal-CT (Op-CT)	[]	4.33 (90)	Op-CT	–
Microcrystalline-	[]	4.12 (100)	Op-CT	–
Pseudocrystalline	[]	3.82 (50)	Op-CT	–
Coarse-grained, Length-fast sometimes Undulotory-damped				
Opalline Quartz Opal-C (Op-C)	[]	2.51 (30)	Op-C	–
Microcrystalline-				
Pseudo-crystalline				
Coarse-grained, Length-fast sometimes Undulotory-damped				

*Ideal XRD data compiled from
– AMCSD, 2011. **American Mineralogist crystal structure database by Downs et al. (1993) *via http://www.minsocam.org/MSA/Crystal_Database.html* and *http://rruff.geo.arizona.edu/AMS/amcsd.php*.**
– WEBMINERAL, 2011. **Minerals arranged by X-Ray powder diffraction *via http://webmineral.com/MySQL/xray.php*.**
– RRUFF, 2011. **Database of Raman spectroscopy, X-ray diffraction and chemistry of minerals *via http://rruff.info/*.**
– ASTM, 1963. **Index (inorganic) to the powder diffraction file; *ASTM special tech. Pub. 48-M2, Am. Soc. for Test. and Mater, Philadelphia, pp. 244.***
– PDF cards-86-1630 (for chalcedony); 46-1045 (for quartz); 38-0360 (for moganite); 38-0448 (for opal).
– Miehe et al., 1984; Miehe and Graetsch, 1992; Murashov and Svishchev, 1998.
*The diffraction matching using the comparative matching technique is based on the positions of peaks with intensities equal and greater than 2% for those of the ideal and the positions of peaks with intensities equal and greater than 2% for those of the sample, having 2-theta values below 70 deg., and tolerance range of ±0.01.

can suggest the silica formation conditions over about 80 °C. In many previously published papers, it has been stated that chalcedonic-quartz precipitations occur in the range between 40 and 150 °C. However, in the microcrystalline quartz occurrences, the coagulations of the kinds of silica building phases depend on the environment conditions. In lower temperature conditions below about 80 °C, opal-CT and opal-C silica building phases appear dominantly. But, in higher temperature conditions above about 180 °C, the moganite (or lutecite) and alpha-quartz silica building phase crystallize (Frondel, 1978; Murashov and Svishchev, 1998; Jones and Segnit, 1971).

3.4. Chemical implications and dispersive confocal micro-Raman vibrational bands

The Biga chrysoprase samples were examined for the first time using dispersive confocal micro-Raman spectroscopy (DCμRS) in combination with X-ray fluorescence (XRF) and inductive coupled plasma-atomic emission spectroscopy (ICP-AES) for analyses and detections. Table 3 shows the average chemical contents. The some of these trace element concentrations are responsible for the production of the Raman bands given in Fig. 6, and many of these vibrational bands are characteristic for the Biga chrysoprases.

The main chemical bulk concentrations of these chrysoprase materials which occur in the silicified serpentinitic host rock are as follows; SiO_2 (95.50%), Al_2O_3 (0.99%), CaO (0.06%), MgO (0.13%), Na_2O (0.12), K_2O (0.18%), and Cr_2O_3 (0.15%). In addition, some trace element concentrations are also very distinctive, such as Fe (13,600 ppm), Ni (4600 ppm), Cr (823 ppm), Pb (417 ppm), Mn (184 ppm), Sb (154 ppm), Zn (192 ppm), and As (126 ppm). Some of these trace elements can be present in any chrysoprase sample from Poland, Kazakhistan, Australia, and Tanzania (Sachanbinski et al., 2001; Skrzypek et al., 2003, 2004), even though the concentrations of some are unusual.

The dispersive confocal micro-Raman (DCμR) spectrum of a representative Biga chrysoprase sample with quartz inclusion in the range between 50 and 1600 cm^{-1} was given in Fig. 6. The spectrum shows that the chrysoprase sample forms from the

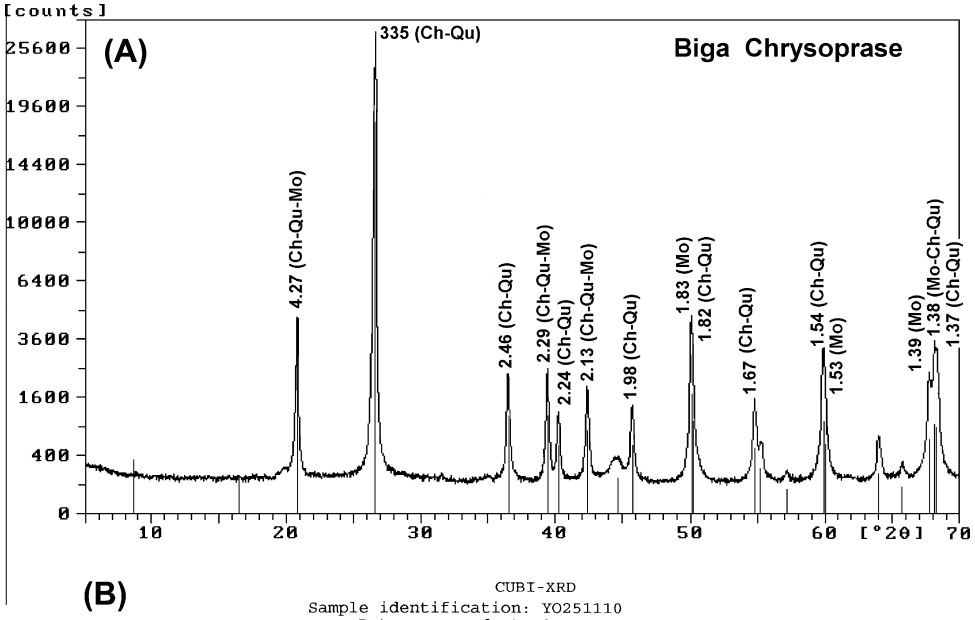

(B)

CUBI-XRD
Sample identification: YO251110
Data measured at: 25-Nov-2010 18:42:00
Tube anode: Cu
Wavelength Alpha1 [Å]: 1.54056
Wavelength Alpha2 [Å]: 1.54439
Start angle [°2θ]: 5.015
End angle [°2θ]: 70.025
Maximum intensity: 17929.21
Intensities converted to: FIXED
Number of peaks: 22

Angle [°2θ]	d-value α1 [Å]	d-value α2 [Å]	Peak width [°2θ]	Peak int [counts]	Back. int [counts]	Rel. int [%]	Signif.
8.700	10.1555	10.1807	0.720	18	335	0.1	0.90
16.500	5.3681	5.3814	0.180	14	154	0.1	0.77
20.830	4.2609	4.2715	0.150	3684	149	20.6	20.86
26.610	3.3471	3.3554	0.180	17929	135	100.0	78.04
36.515	2.4587	2.4648	0.180	1043	71	5.8	17.45
39.430	2.2834	2.2891	0.180	1050	59	5.9	15.37
40.245	2.2390	2.2446	0.210	480	58	2.7	12.83
42.415	2.1293	2.1346	0.180	751	53	4.2	13.35
44.665	2.0272	2.0322	0.240	92	50	0.5	1.39
45.750	1.9816	1.9865	0.210	488	48	2.7	14.26
50.090	1.8196	1.8241	0.150	1616	45	9.0	12.04
50.225	1.8150	1.8195	0.060	955	45	5.3	4.44
54.825	1.6731	1.6773	0.150	467	42	2.6	5.83
55.275	1.6605	1.6647	0.150	199	44	1.1	2.03
57.210	1.6089	1.6129	0.240	24	44	0.1	1.51
59.900	1.5429	1.5467	0.180	949	46	5.3	13.72
60.085	1.5386	1.5424	0.090	529	46	3.0	0.80
63.985	1.4539	1.4575	0.210	149	42	0.8	7.16
65.710	1.4198	1.4234	0.180	42	44	0.2	1.68
67.685	1.3831	1.3866	0.150	600	45	3.3	5.33
68.095	1.3758	1.3792	0.120	906	46	5.1	3.20
68.215	1.3737	1.3771	0.120	847	45	4.7	2.80

Fig. 5. The XRD pattern of the representative Biga chrysoprase (A), according to the numerical experimental XRD data (B), showing the labels of the single or overlapped peaks of the base microcrystalline and crystalline silica building phase components. These are fibrous chalcedony (optically length-fast) (Ch), fibrous moganite (optically length-slow) (Mo), and fine-grained alpha-quartz (optically length-fast) (Qu). The positions of peaks with d-spacings [Å] and relative intensities [%(I/I_o)] are labeled for ⩾2% of 2-theta values below 70°. The labels of overlapped peaks are in order of relative intensities [%(I/I_o)].

chalcedonic-quartz silica building phase (fibrous chalcedony) dominantly. Additionally, the spectra in Figs. 7 and 8 show a combination of the mapped Raman spectra and related microscope images, and also the overlapped and separated Raman spectra which were compared with that of ideal fibrous chalcedony, respectively.

On the other hand, in the same deposit, the massive green-stained quartz masses are also present, and they are common and have a low-quality in terms of gemmological importance. Thus, it is necessary to distinguish these masses from each other non-destructively. Dispersive confocal micro-Raman spectroscopy (DCμRS) help to clearly distinguish the chalcedonic-quartz silica building phase (fibrous chalcedony) from the crystalline-quartz silica building phase (fine-grained alpha-quartz) in both chrysoprase and green-stained quartz masses in this deposit. The representative Raman spectrum of the massive green-stained quartz mass was given in Fig. 9, and the overlapped and separated Raman spectra which were compared with that of ideal quartz were given in Fig. 10.Ultimately, in order to compare these two Raman spectra, the combined Raman spectra showing the chalcedonic-quartz silica phase and the crystalline-quartz silica phase (Figs. 6 and 9) were given in Fig. 11.

It is important to note that these Raman bands of Biga chrysoprase have not been reported in any previous references. Therefore, these first experimental data (Table 4) of the chrysoprase samples indicate that the formation of distinctive vibrational bands is definitely related to lattice defects, which can be attributed to some chemical impurities (external defects) and structural imperfections (internal defects).

A total of 14 vibrational Raman bands of the Biga chrysoprase were established, and their causes were inferred regarding some crystalline lattice defects (Table 4). However, five of these bands

Table 3
Average bulk and trace element chemical analyses of the representative Biga chrysoprase sample. Relatively higher concentrations of trace elements, such as Fe, Cr, Mn, As, Ni, Pb, Sb, and Zn are unique characteristics of the Biga chrysoprase. Some of them are certainly responsible for the production of both the characteristic green color (mainly nickel) and the confocal micro-Raman vibrational bands.

Oxides %	Instrument (XRF) Detection limits	Sample Biga chrysoprase	Elements	Instrument (ICP–AES) Detection limits	Sample Biga chrysoprase
SiO_2	0.01%	95.50			
Al_2O_3	0.01%	0.99	Al	0.01%	0.54
Fe_2O_3	0.01%	1.98	Fe	0.01%	1.36
CaO	0.01%	0.06	Ca	0.01%	0.06
MgO	0.01%	0.12	Mg	0.01%	0.04
Na_2O	0.01%	0.13	Na	0.01%	0.03
K_2O	0.01%	0.18	K	0.01%	0.13
Cr_2O_3	0.01%	0.15	Cr	1 ppm	823
TiO_2	0.01%	0.02	Ti	0.01 ppm	0.01
MnO	0.01%	0.03	Mn	5 ppm	184
P_2O_5	0.001%	0.013	P	10 ppm	20
SrO	0.01%	0.01	Sr	1 ppm	17
BaO	0.01%	0.01	Ba	10 ppm	20
LOI	0.01%	0.64			
Total	0.01%	99.83			
			Ag	0.5 ppm	2.5
			As	5 ppm	126
			Be	0.5 ppm	<0.5
			Bi	2 ppm	<2
			Cd	0.5 ppm	0.8
			Co	1 ppm	4
			Cu	1 ppm	13
			Ga	10 ppm	<10
			La	10 ppm	<10
			Mo	1 ppm	2
			Ni	1 ppm	4600
			Pb	2 ppm	417
			S	0.01 ppm	0.01
			Sb	5 ppm	154
			Sc	1 ppm	1
			Th	20 ppm	<20
			Tl	10 ppm	<10
			U	10 ppm	<10
			V	1 ppm	8
			W	10 ppm	<10
			Zn	2 ppm	192

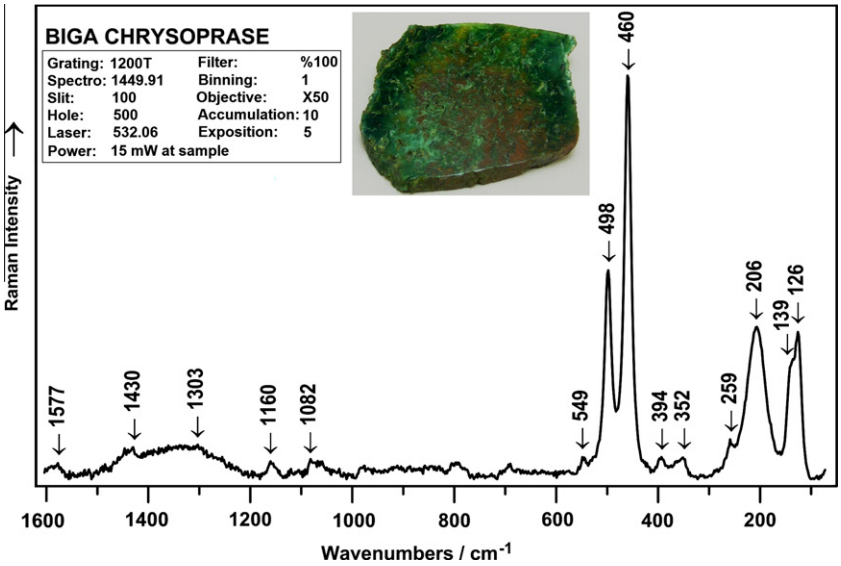

Fig. 6. The dispersive confocal micro-Raman vibrational bands in the Biga chrysoprase spectrum representing microcrystalline chalcedonic quartz.

peaked at 498, 460, 206, 139, and 126 cm^{-1} are distinctive because of the remarkable differences of the relative intensities and positions of the peaks (Fig. 6).

The most recent technological developments in Raman spectroscopy have enabled rapid mapping (Gouadec and Colomban, 2007; Colomban and Prinsloo, 2009; Carter et al., 2010). Rapid

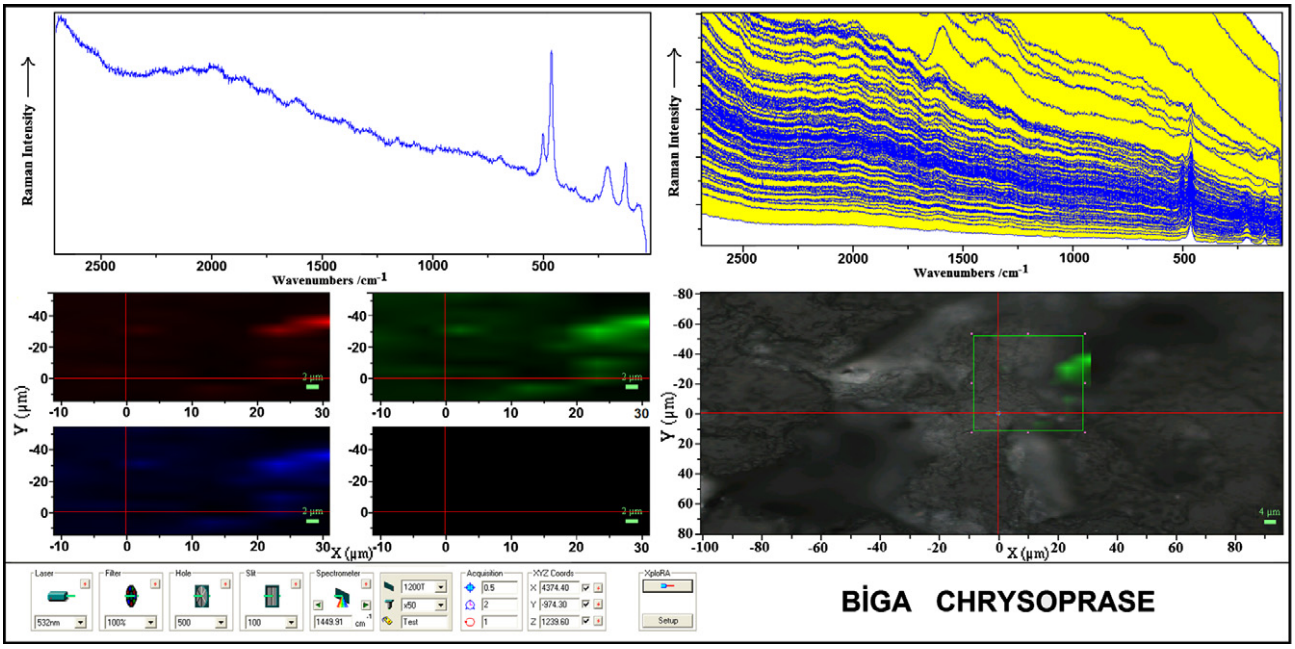

Fig. 7. The mapped multi spectra and related microscope image of Fig. 6. They show the variation of any fitted parameter (i.e. intensity, width or position of one band) as a function of the point of analysis. If the mapping is regular and sufficiently tight, one gets a "smart map" of the parameter (color or contrast scaling) superimposed with the optical image of the probed area.

mapping capabilities allow the large scale survey maps to be collected first and smaller, higher spatial resolution maps obtained once a region of interest has been located. The large scale map and the related microscope images of the Biga chrysoprase suggest the existing of the same bands (Fig. 7).

Finally, the obtained bands in the spectrum of the Biga chrysoprase were matched with the bands in the spectrum of ideal chalcedony both in the spectrometer library and in the well-known database (RRUFF, 2011). Comparison and contrast of these Raman bands show that the bands of the Biga chrysoprase are highly

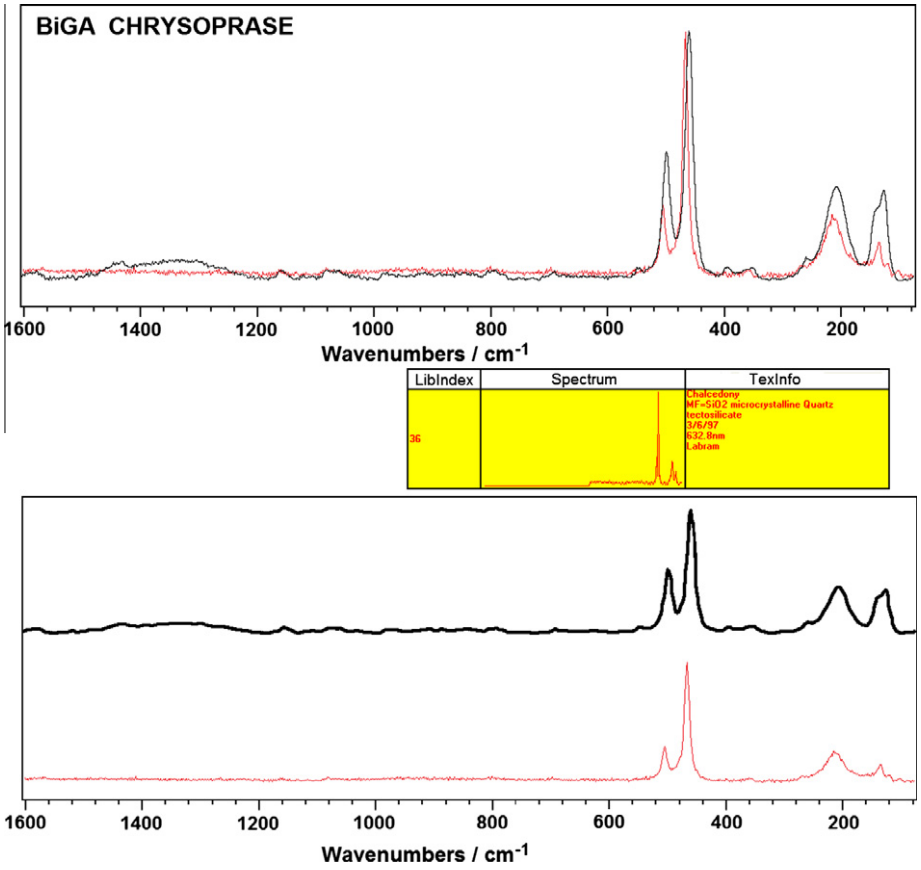

Fig. 8. A comparison with those of ideal fibrous chalcedony of the dispersive confocal micro-Raman bands of fibrous chalcedony in the Biga chrysoprase.

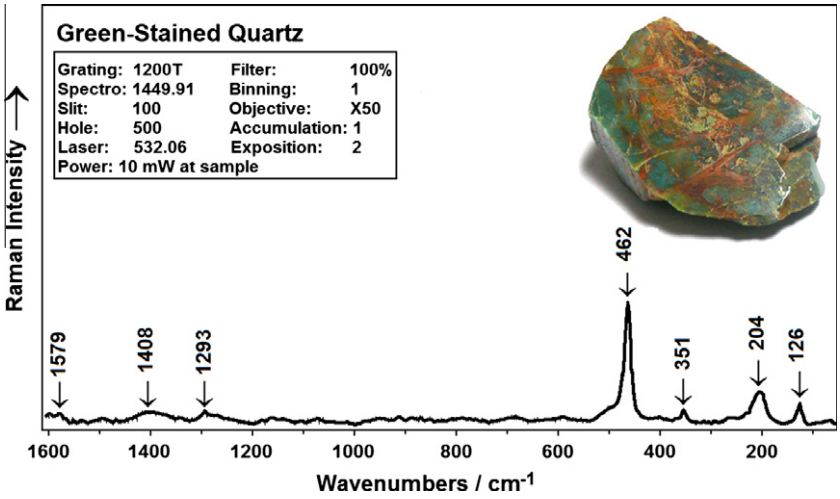

Fig. 9. The dispersive confocal micro-Raman vibrational bands in the spectrum of the green-stained quartz mass, found in the same deposit. It is common and in low-quality in terms of gemmological importance.

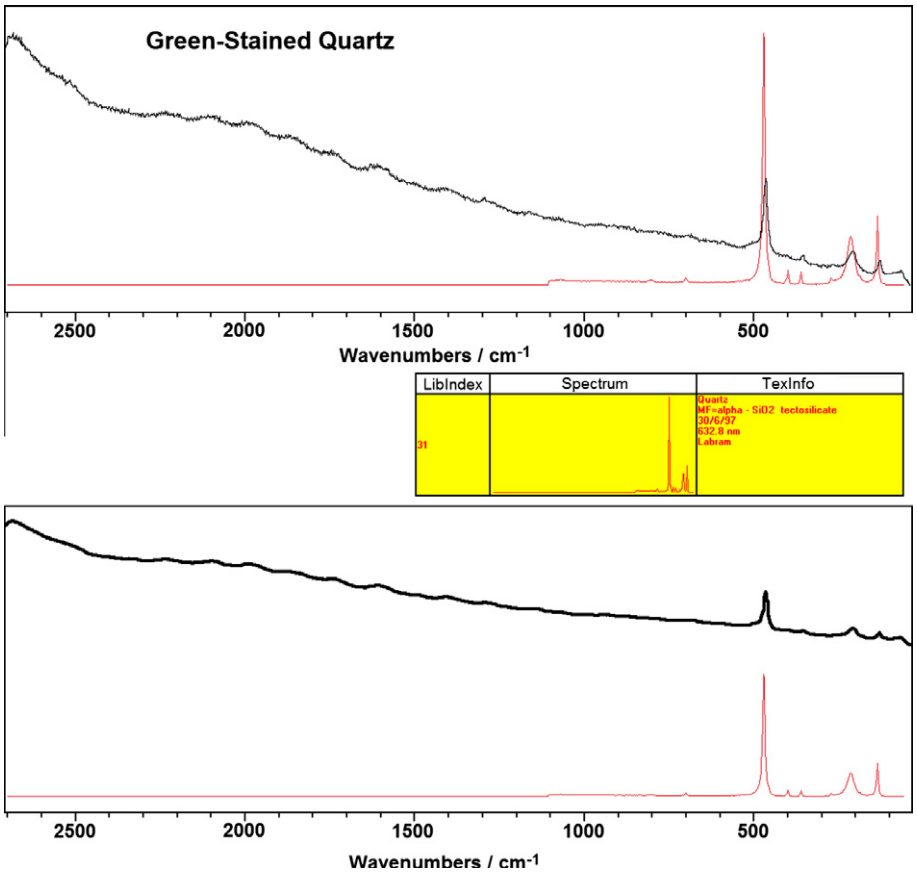

Fig. 10. A comparison with those of ideal fine-grained alpha-quartz of the dispersive confocal micro-Raman bands in the green-stained quartz.

similar to those of ideal chalcedony, which form the microcrystalline chalcedonic-quartz texture (Fig. 9).

All collective vibrations in the crystals can be viewed as the superposition of plane waves that virtually propagate to infinity. These plane waves (the normal modes of vibration) are commonly modeled by quasi-particles called photons. A normal coordinate of the form $Q = Q_o \cos(2\pi\nu n_{vib} t)$, which is actually a linear combination of bond lengths and bond angles, is associated with each normal mode. Depending on the dominant term in the normal coordinate, these modes can be classified as either stretching (n), bending (d), torsional (t), librational (R_0/T_0 pseudorotations/translations) or lattice modes (the latter include the relative displacement of the unit cells) (Vandenabeele, 2010; Slodczyk and Colomban, 2010; Gouadec and Colomban, 2007; Colomban and Prinsloo, 2009).

Table 3 shows that the relatively higher concentrations of some transition metal elements, such as Fe, Ni, Cr, Mn, Pb, and Zn are characteristic for the Biga chrysoprases.

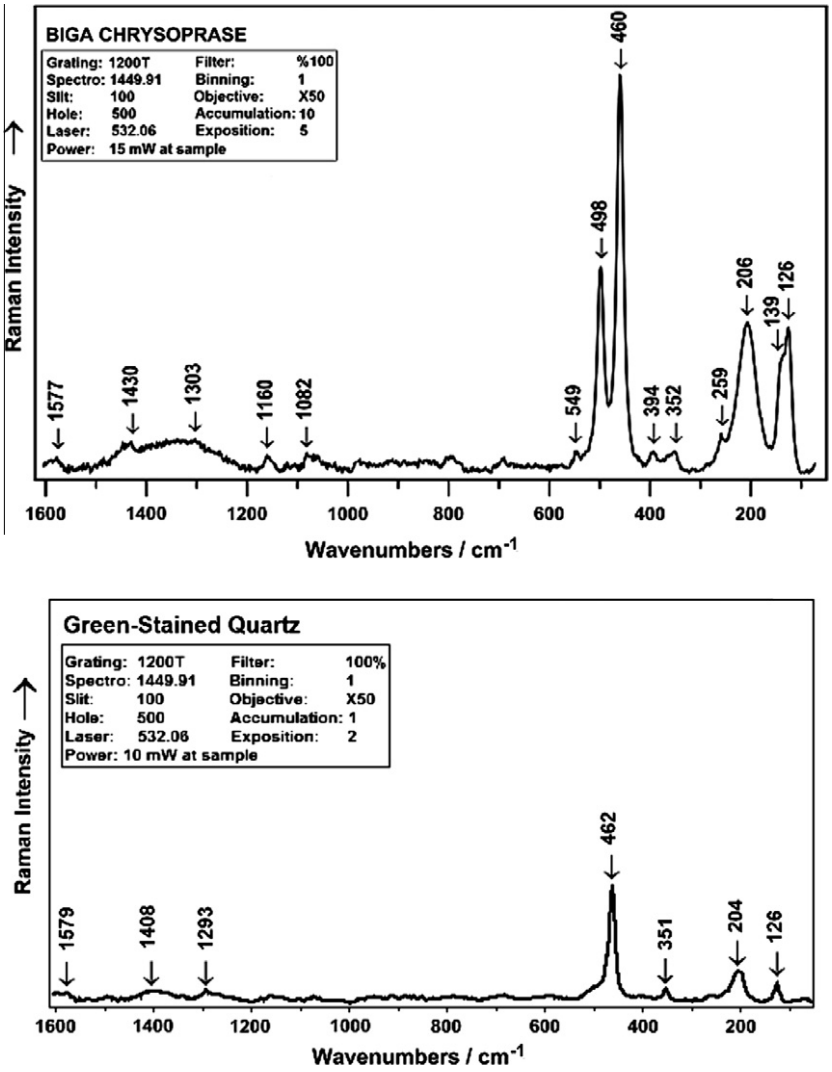

Fig. 11. Combined Raman spectra of chalcedonic-quartz and crystalline-quartz, seen in Figs. 6 and 9.

Table 4
Confocal micro-Raman vibrational bands of the representative Biga chrysoprase, and their inferred causes according to symmetry and Raman activity of SiO_4 tetrahedron with Td symmetry (the inferences were modified from Colomban and Prinsloo, 2009).

Peak number	Micro-Raman bands wavenumbers (cm^{-1})	Inferred causes
1	1577	Single nonbridging oxygen hole centers with several precursors (i.e., hydroxyl group, peroxy linkage) and oxygen vacancy
2	1430	Doubly nonbridging oxygen hole centers with several precursors (i.e., hydroxyl group, peroxy linkage) and oxygen
3	1303	vacancy
4	1160	ν_1 doubly symmetric stretching modes of degeneracy of [SiO_4/M] centers
5	1082	
6	549	ν_1 single symmetric stretching modes of degeneracy of [SiO_4/M] centers
7	498	ν_2 doubly symmetric bending mode of [SiO_4/M] centers. The "M" includes the some cationic substitutions of Si by Fe, Cr,
8	460	Mn, As, Ni, Pb, Sb, and Zn, and also K and Na
9	394	ν_4 doubly asymmetric bending modes of degeneracy of [SiO_4/M] centers
10	352	
11	259	Single rotational libration mode
12	206	Single translational libration mode
13	139	Doubly translational libration modes
14	126	

The production of Raman bands of the Biga chrysoprases can be mainly attributed to extrinsic defects (chemical impurities), which are due to increasing amounts of tetrahedral character with increasing electron density caused by the presence of trace elements, taking into consideration the increased ionic character of the Si–O and Al–O bonds in the alkali silicate (Weil, 1984), and can be partially attributed to intrinsic defects (the nonbridging oxygen deficient centers with several precursors and self-trapped excitation).

Nutall and Weil (1980) reported a hydrogenic trapped hole-center with four hydrogen atoms in a regular silicon lattice position. Since, in the case of some elements, a compensation of the

electric charge is necessary, additional cations such as H, Li, Na., K, and Ag can be incorporated in inter-lattice positions in conjunction with structural channels. The nonbridging oxygen hole center (≡Si–O) is described as a hole trapped in a single oxygen atom bound to a single silicon on three oxygen atoms in the SiO_2 structure (Weil, 1984). Oxygen excess centers include the peroxy radical (≡Si–O–O), the hole centers consisting of an O^{2-} ion bonded to single silicon on three oxygen atoms, and the peroxy linkage (≡Si–O–O≡). A further type of defect is OH^- centers which consist of a proton bound on a regular lattice O^{2-} ion, located between two O^{2-} ions of the SiO_4 tetrahedron. Because of the negative net charge, additional trivalent substitutes of the Si^{4+} positions occur as the charge compensation (i.e. Al^{3+}) in such a way that an additional proton is bound on the Al^{3+} (Vandenabeele, 2010; Gouadec and Colomban, 2007; Colomban and Prinsloo, 2009).

However, the contribution of ionic bonds like Al-O is null according to that of covalent Si-O bonds (Colomban and Prinsloo, 2009). So, the considerable strength of the Si–O bond results in a high melting temperature (Colomban and Prinsloo, 2009). The basic unit of a silicate, the SiO_4 tetrahedron, is a strong chemical entity and the possibility to share oxygen atoms between two tetrahedra with variable Si–O–Si angles or to have non-bridging oxygen atoms gives a polymeric character to silicates (Colomban and Prinsloo, 2009). The $[SiO_4]^\circ$ center is caused by substitution for Si^{4+} with an electron hole at one of the four nearest O^{2-} ions, forming O^-.

Slodczyk and Colomban (2010) have stated that many electrical / electrochemical/magnetic properties result from a competition between different potentials of the chemical bonding and structure. In general, some atoms (alkali and earth alkali cations) have a strong ionic character. Some other atoms develop covalent bonding (i.e., transition metals) and form strong "molecular" bricks. Metallic bonds can also be formed between atoms such as Ag, Cu, Tl, and ionized clusters intermediately between ions and complex nano-clusters may be observed (Slodczyk and Colomban, 2010).

Gouadec and Colomban (2007) have stated that the width of the other Raman modes is mainly sensitive to the "local" crystal field, more specifically to the short range order in the first (0.1–0.5 nm) and second (0.5–5 nm) atomic shells. If the "molecular" description of vibrations applies, then Raman bending modes are even specifically sensitive to local geometric disorientation and Raman stretching modes to the neighboring disorder (particularly atoms from other sub-lattices or electric defects resulting from substitutions/vacancies) (Gouadec and Colomban, 2007).

It can be seen that a dispersive confocal micro-Raman spectrometer (DCμRS) can be reliably used to identify many silica varieties in terms of the constitutive and inclusion silica building phases.

It was observed using X-ray diffractometry and polarizing microscopy that the gem-quality dark green chrysoprase masses in the Biga–Çanakkale region mainly composed of the chalcedonic-quartz main silica building phase (fibrous chalcedony), as well as inclusions of the chalcedonic-quartz interval silica building phase (fibrous moganite) and the crystalline-quartz main silica building phase (fine-grained alpha-quartz). Even though these base silica building phases can be easily identified in thin sections under a polarizing microscope, the fibrous chalcedony phase cannot be clearly distinguished from the fine-grained alpha-quartz phase using X-ray diffractometry, since they exhibit the same numerical XRD data.

After the dispersive confocal micro-Raman spectroscopy (DCμRS) had been performed on these chrysoprases, it was seen that the fibrous chalcedony silica phase representing the chalcedonic-quartz structure could be quickly and non-destructively distinguished from the fine-grained alpha-quartz silica phase representing the rystalline-quartz structure. However, this procedure could not be carried out on the interval moganite silica phase representing the other crystalline-quartz structure, since the ideal Raman spectrum of moganite is not present in the databases yet.

The mainly dark green coloration of the Biga chrysoprases is due to a complex mechanism, since many transition metals, which are coloration agents, are present. Some of the elements Fe, Cr, Mn, As, Ni, Pb, Sb, and Zn are certainly responsible for the coloration as the external lattice defects. However, nickel is the main ion for producing the dark green color (Nagase et al., 1997; Sachanbinski et al., 2001; Witkowski and Zabinski, 2004; Befi, 2009; Shigley et al., 2009). Some trace elements, such as iron and chromium ions modify the typical green color with an adding brownish hue of the chrysoprases, but in order to clarify this colororation mechanism, further investigations will be necessary.

Nagase and his colleagues (1997) have tried to identify the origin of the green color in the chrysoprases from Warrawanda, Western Australia. Their TEM observations and IR-spectra analyses show that the chrysoprases include kerolite, which occurs as a cotton-like aggregate of extremely fine-grained crystals at the boundaries of coarse grains in the quartz crystals. Their EPMA analyses show that the kerolite contains about 10 wt% NiO, and that NiO content of the chrysoprase increases with the degree of silicification of the surrounding serpentinite. The Ni-bearing kerolite derived from the silicified serpentinite is inferred to production of the typical green color of the chrysoprases (Nagase et al., 1997).

Ultimately, it can be stated that some (mainly nickel) of the trace elements found in this study are certainly responsible for the production of both the characteristic green color and the Raman vibrational bands.

4. Conclusions

This study characterizes the Biga chrysoprase from Turkey, defining its constitutive silica building phases, using several destructive and non-destructive analytical techniques. Polarizing microscopic examination reveals that the chrysoprases consist of fibrous silica matrixes and centrally located inclusions of crystalline silica. The identification of these silica phases was also confirmed by X-ray powder diffraction data using the comparative matching technique. However, opalline-quartz (opal-CT and opal-C) silica building phases do not exist in these chrysoprase samples. Because of the existing of the chalcedonic-quartz silica interval phase (moganite) instead of the opalline-quartz silica base phase (opal-CT and opal-C), it can be stated that the Biga chrysoprases from Turkey occur relatively higher formation temperature conditions, and this structural feature distinguish the Biga chrysoprase from the other chrysoprases from Poland, Kazakhstan, Australia, Brazil, and Tanzania.

The matrix investigation methods (polarizing microscopy, X-ray diffraction and X-ray fluorescence spectroscopies) in the minerals are destructive and/or invasive, and thus, they are not used for identifying ancient and/or actual gem-mineral objects. On the contrary, the non-destructive and/or non-invasive advantage of the micro-Raman spectroscopy is very usable for these kinds of gem materials, especially in distinguishing the alpha-quartz phase from the chalcedony, opal-CT, and opal-C phases. In addition, this method can be reliably used to distinguish all kinds of microcrystalline chalcedonic-quartz varieties (i.e. chrysoprase, blue chalcedony, agate, etc.) from all kinds of crystalline quartz varieties (i.e. rock crystal, citrine, smoky quartz, amethyst, etc.).

The characterizations on the chrysoprase material -from the bulk chrysoprase producer countries (Poland, Kazakhstan, Australia, Brazil, and Tanzania) – has been significantly supplemented by many authors using different characterization techniques, such

as UV–Vis, XRD, FT-IR, EPMA, TEM, EPR, and TPR, for the last 30 years. However, the chrysoprase material from the Biga–Çanakkale region of Turkey which is the newest producer country in the world was characterized for the first time in this study in terms of its silica building phases, using several destructive (polarizing microscope, XRD, XRF and ICP-AES) and non-destructive (hydrostatic balance, refractometer, UV-luminescence, and DCμRS) analytical techniques.

It is seen that DCμRS can be reliably used to identify the silica mineral species regarding to their main silica building phases. Single and mapped confocal micro-Raman spectra were compared and contrasted with those of the ideal micro-Raman bands in fibrous chalcedony and fine-grained alpha-quartz spectra. The rapid mapping capabilities allow the large scale survey maps to be collected with smaller higher spatial resolution maps obtained once a region(s) of interest has been located. This technology has been used to investigate the Biga chrysoprase.

It is well-known that chrysoprase contains nickel ions; the nickel is what gives the color of the chrysoprases. However, ICP-AES results show that the remarkable abundance of chromium can play an important role in the production of dark green coloration of Biga chrysoprases.

Acknowledgements

This study is a part of the thesis prepared for the B.Sc., by the second author. The confocal micro-Raman spectrometer used in this study was purchased with the grant of the BAP Project, No. BAP-2009.KB.FEN.051, of Dokuz Eylül University. Accordingly, the authors wish to give great thanks to Prof. Dr. R. Sami AKSOY, Prof. Dr. İ. Hakkı BAHAR, Cengiz HEPİYİLER, and Prof. Dr. Necdet TÜRK for their help and support during the purchasing procedure of the spectrometer, and also to Instructor Helen Margaret MORAN-ÇAĞLAR from Dokuz Eylül University, School of Foreign Languages, for proof-reading the manuscript, and ultimately to referees' for constructive review, recommendations, and patience.

References

AMCSD, 2011. American Mineralogist crystal structure database by Downs et al. (1993) *via.* <http://www.minsocam.org/MSA/Crystal_Database.html and http://rruff.geo.arizona.edu/AMS/amcsd.php>.

ASTM, 1963. Index (inorganic) to the powder diffraction file; ASTM special tech. Pub. 48-M2, Am. Soc. for Test. and Mater, Philadelphia. pp. 244.

Arem, J.E., 1987. Color Encyclopaedia of Gemstones, 2nd ed. Van Nostrand Reinhold. Co., New York, pp. 248.

Back, M., Mandarino, J., 2008. Fleischer's Glossary of Mineral Species, 10th ed. The Mineralogical Record, Inc., Tucson, pp. 345.

Befi, R., 2009. Australian chrysoprase with dendritic inclusions. Gems & Gemology 45, 71.

Bersani, D., Lottici, P.P., 2008. Application of Raman spectroscopy to gemology. Analytical and Bioanalytical Chemistry 397, 2631–2646.

Bingöl, E., Akyürek, B., Korkmazer, B., 1973. Biga yarımadasının jeolojisi ve Karakaya Formasyonunun bazı özellikleri. In: Proceedings of the 50th Anniversary of the Turkish Republic Earth Science Congress, Mineral Research and Exploration Institute of Turkey (MTA) Publications, pp. 70–77 (in Turkish).

Cady, S.L., Wenk, H.R., Sintubin, M., 1998. Microfibrous quartz varieties: characterization by quantitative X-ray texture analysis and transmission electron microscopy. Contributions to Mineralogy and Petrology 130, 320–335.

Caillaud, J., Proust, D., Philippe, S., Fontaine, C., Fialin, M., 2009. Trace metals distribution from a serpentinite weathering at the scales of the weathering profile and its related weathering microsystems and clay minerals. Geoderma 149, 199–208.

Carter, E.A., Pasek, M.A., Smith, T., Kee, T.P., Hines, P., Edwards, H.G.M., 2010. Rapid Raman mapping of a fulgurite. Analytical and Bioanalytical Chemistry 397, 2647–2658.

Colomban, P., Prinsloo, L., 2009. Optical spectroscopy of silicates and glasses. In: Yatwood, J., Douthwaite, R., Duckett, S. (Eds.), Spectroscopic Properties of Inorganic and Organometallic Chemistry, vol. 40. RSC Publishing, pp. 128–149.

Deckert, V., George, M.W., Umapathy, S., 2008. Raman spectroscopy at the beginning of the twenty-first century II. Journal of Raman Spectroscopy 39, 1508–1511.

Fana, J.L., Guoa, S.G., Liua, X.L., 2009. The Application of confocal micro-Raman spectrometer to nondestructive identification of filled gemstones. Spectroscopy Letters 42, 129–135.

Frondel, C., 1978. Characters of quartz fibers. American Mineralogist 63, 17–27.

Gouadec, G., Colomban, P., 2007. Raman Spectroscopy of nanomaterials: how spectra relate to disorder, particle size and mechanical properties. Progress in Crystal Growth and Characterization of Materials 53, 1–56.

2009. Micro-Raman spectroscopy and luminescence studies in the earth and planetary sciences. In: Gucsik, A. (Ed.), Proceedings of the International Conference Spectroscopy 2009, Mainz, Germany, 2–4 April, 2009, pp. 1163 (p. 250).

Jones, J.B., Segnit, E.R., 1971. The nature of opal I. Nomenclature and constituent phases. Australian Journal of Earth Sciences 18, 57–68.

Koçyiğit, A., Bozkurt, E., Deveci, Ş. 2006. The Transition zone between the Extensional and Strike-slip neotectonic regimes in southern Marmara region: Bursa Graben. In: International Workshop on Comparative studies of the NAF (NW Turkey) and the SAF, Southern Californi, vol. 1, pp. 18–19.

Komov, I.L., Lukashev, A.N., Koplus, A.V., 1994. Geochemical methods of prospecting for non-metalic minerals. VSP BV, The Netherlands. 185.

Lewis, I.R., Edwards, H.G.M., 2001. Handbook of raman spectroscopy, from the research laboratory to the process line. Practical Spectroscopy Series. Marcel Dekker Inc.,, New York..

Miehe, G., Graetsch, H., Flörke, O.W., 1984. Crystal structure and growth fabric of length-fast chalcedony. Physics and Chemistry of Minerals 10, 197–199.

Miehe, G., Graetsch, H., 1992. Crystal structure of moganite: a new structure type for silica. European Journal of Mineralogy 4, 693–706.

Murashov, V.V., Svishchev, I.M., 1998. Quartz family of silica polymorphs: comparative simulation study of quartz, moganite, and orthorhombic silica, and their phase transformations. Physical Review B: Condensed Matter 57, 5639–5646.

Nagase, T., Akizuki, M., Onoda, M., Sato, M., 1997. Chrysoprase from Warrawanda, Western Australia. Neues Jahrbuch für Mineralogie Monatshaft 7, 289–300.

Nutall, R.H.D., Weil, J.A., 1980. Two hydrogenic trapped-hole species in quartz. Solid State Communications 33, 99–102.

Okay, A.I., Siyako, M., Bürkan, B.A., 1991. Geology and tectonic evolution of the Biga Peninsula, northwest Turkey. Bulletin of the Technical University of Istanbul 44, 191–256.

Okay, A.I., Satır, M., 2000. Upper cretaceous eclogite-facies metamorphic rocks from the Biga Peninsula Northwest, Turkey. Turkish Journal of Earth Sciences 9, 47–56.

Sachanbinski, M., Janeczek, J., Platonov, A., Rietmeijer, F.J.M., 2001. The origin of colour of chrysoprase from Szklary (Poland) and Sarykul Boldy (Kazakhstan). Neues Jahrbuch für Mineralogie Abhandlungen 177, 61–76.

Rossman, G.R., 1994. Colored varieties of the silica minerals. Silica: Physical Behavior, Geochemistry and Materials Applications 29, 433–467.

RRUFF, 2011. Database of Raman spectroscopy, X-ray diffraction and chemistry of minerals *via.* <http://rruff.info/>.

Shigley, J.E., Laurs, B.M., Renfro, N.D., 2009. Chrysoprase and prase opal from Haneti, central Tanzania. Gems & Gemology 45, 271–279.

Skrzypek, G., Sachanbinski, M., Jedrysek, M.O., 2003. Oxygen isotope evidence for low temperature formation of chrysoprase. Polskie Towarzystwo Mineralogiczne–Prace Specjalne Mineralogical Society of Poland–Special Papers, Zeszyt 22, 2003, pp. 204–206.

Skrzypek, G., Jedrysek, M.O., Sachanbinski, M., 2004. Oxygen stable isotope geochemistry of chrysoprase from wiry and Szklary Mines (SE Poland). In: Conference papers of International Symposium on Isotope Hydrology and Integrated Water Resources Management, 19–23 May 2003, Vienne, Austria, pp. 470–472.

Slodczyk, A., Colomban, P., 2010. Probing the nanodomain origin and phase transition mechanisms in (un) poled PMN-PT single crystals and textured ceramics. Materials 3, 5007–5029.

Smith, D.K., 1997. Evaluation of the detectability and quantification of respirable crystalline silica by X-ray powder diffraction. Powder Diffraction 12, 200–227.

Wang, A., Han, J., Guo, L., Yu, J., Zeng, P., 1994. Database of standard Raman spectra of minerals and related inorganic crystals. Applied Spectroscopy 48, 959–968.

WEBMINERAL, 2011. Minerals arranged by X-ray powder diffraction via http://webmineral.com/MySQL/xray.php.

Weil, J.A., 1984. A review of electron spin spectroscopy and its application to the study of paramagnetic defects in crystalline quartz. Physics and Chemistry of Minerals 10, 149–165.

Witkowski, S., Zabinski, W., 2004. Application of the TPR method for the studies of Ni(II) in chrysoprase. Journal of Thermal Analysis and Calorimetry 77, 143–149.

Vandenabeele, P., 2010. Raman spectroscopy. Analytical and Bioanalytical Chemistry 397, 2629–2630.